Chinese Journal of Aeronautics, (2024), 37(6): 392–409

Chinese Society of Aeronautics and Astronautics
& Beihang University

Chinese Journal of Aeronautics

cja@buaa.edu.cn
www.sciencedirect.com

FULL LENGTH ARTICLE

Temperature field characteristics of CF/PEEK thermoplastic composites formed by automated fiber placement using hot gas torch with slit structure nozzle

Ziang JIN [a,b], **Shouzheng SUN** [a], **Sunil Chandrakant JOSHI** [b], **Zhenyu HAN** [a,*], **Hongya FU** [a]

[a] *State Key Laboratory of Robotics and System, Harbin Institute of Technology, Harbin 150001, China*
[b] *School of Mechanical and Aerospace Engineering, Nanyang Technological University, Singapore 639798, Singapore*

Received 30 May 2023; revised 29 June 2023; accepted 13 August 2023
Available online 2 April 2024

KEYWORDS

Fiber reinforced plastics;
Thermoplastics;
Heating temperature;
Automated fiber placement;
CF/PEEK

Abstract *In-situ* consolidation forming of high-performance thermoplastic composites by Automated Fiber Placement (AFP) is of significant interest in aerospace. During the laying process, the heating temperature has a great influence on the quality of the formed components. A three-dimensional heat transfer finite element model of Carbon Fiber (CF)/Polyether Ether Ketone (PEEK) heated by Slit Structure Nozzle Hot Gas Torch (SSNHGT) assisted AFP is proposed. The influence of gas flow rate, heat transfer distance, and laying speed on heating temperature is analysed. The results show that the overall temperature increases and then decreases as the gas flow rate increases. With the increase in heat transfer distance and laying speed, the overall temperature decreases. Meanwhile, the gas flow rate has the greatest influence on the temperature of CF/PEEK being heated, followed by the laying speed and finally the heat transfer distance. Furthermore, the model can also be extended to other fiber-reinforced polymer composites formed by hot gas torch assisted AFP, which can guide the optimization of process parameters for subsequent heating temperature control.

1. Introduction

Compared to thermoset composites, thermoplastic composites are attractive in aerospace components for their high fracture toughness, high damage tolerance, no shelf-life effect on manufacturing, weldability, and recyclability.[1,2] As an advanced automated composites forming technique, Automated Fiber Placement (AFP) has the advantages of high production

* Corresponding author.
E-mail address: hanzy@hit.edu.cn (Z. HAN).
Peer review under responsibility of Editorial Committee of CJA.

https://doi.org/10.1016/j.cja.2024.03.032

efficiency, low material waste, and the ability to form complex curved components.[3,4] Furthermore, AFP can form thermoplastic composites by *in-situ* consolidation, which further reduces processing steps and production costs.[5,6] Therefore, the technique of AFP *in-situ* forming thermoplastic composites is attractive to the aerospace industry.

However, for Carbon Fiber (CF)/Polyether Ether Ketone (PEEK) thermoplastic composites with high melting points and high viscosity,[7] the mechanical performance of CF/PEEK laminates made by the AFP *in-situ* consolidation process cannot meet the requirements of the aerospace industry due to the rapid heating and cooling characteristics. Unreasonable process parameters in the AFP process seriously affect the mechanical properties of the laminates. For example, Qureshi et al.[8] found that increasing the mold temperature could reduce the temperature gradient between the feed tape and the substrate, resulting in CF/PEEK laminates with better interlaminar shear strength and fracture toughness. Comer et al.[9] found that the laying speed of AFP was so fast that the prepreg could not be completely melted along the thickness direction. The formed CF/PEEK laminates had low crystallinity and more voids, which severely impaired the mechanical performance. Bandaru et al.[10] found that laser power had a significant effect on the mode I fracture toughness of CF/PEEK laminates, while it had less effect on the mode II fracture toughness. The temperature distribution during the laying process is one of the most important factors affecting the mechanical performance of the laminates. Uneven temperature distribution causes changes in the characteristics of the material (e.g., density, crystallinity), which in turn causes the generation of residual stresses and deformations.[11] The heating methods for AFP mainly include a hot gas torch, laser, and infrared heaters, in which hot gas torch or laser is commonly used as the heat source for CF/PEEK thermoplastic composites.[12–14] In recent years, the laser has been widely used in AFP forming thermoplastic composites due to the faster processing rates, high energy density, and more focused and more effective heating.[15] However, it also has some disadvantages, including safety issues involved with the implementation of laser, difficulty in controlling the precise location of the end of the beam, and the limitation of laser for glass fiber reinforced polymer composites.[16,17] Compared with laser, hot gas torch is also widely used in AFP because it can avoid all the disadvantages of laser despite the disadvantages of low thermal efficiency.[18–20]

Studies on heat transfer models for thermoplastic composites made by hot gas torch assisted AFP have included one-dimensional,[21,22] two-dimensional,[23,24] and three-dimensional models.[25] Tierney[26] studied a one-dimensional heat transfer model for hot gas torch assisted AFP. The model only considered the single point temperature in the thickness direction, neglecting the temperature distribution in the length and width directions. Toso et al.[27] constructed a two-dimensional transient heat transfer model using the finite element method. The temperature distribution gradients and convective heat transfer coefficients were obtained by comparing the simulation results with the experimental results. Li et al.[28] used the element birth and death technique in ANSYS to simulate the transient temperature field in the thermoplastic tape lay-up process to obtain the temperature distribution along the thickness direction. However, the model was not validated by experiments. Tafreshi et al.[29] created a two-dimensional transient heat transfer model using the finite difference method. The results showed that although the maximum temperature values obtained from the simulations agreed with the experimental results, the theoretical curves did not follow the experimental curves due to many simplifications such as neglecting the thermal contact resistance, thermal conductivity, and specific heat capacity. Moghadamazad and Hoa[30] developed a two-dimensional transient heat transfer analysis considering the interlayer thermal contact resistance and temperature dependence of the material properties. The validity of the heat transfer model was verified by comparing the theoretical results with the experimental results. Kim et al.[25] used the finite element method to develop a three-dimensional heat transfer model of AFP. The distribution of convective heat transfer coefficients on the composite surface was obtained by analysing the hot gas flow in the area between the feed tape and the composite substrate. Hassan et al.[31] constructed a three-dimensional transient heat transfer model. In this model, the final convective heat transfer coefficient was obtained by modifying the heat transfer coefficient through an iterative process to make the simulation results consistent with the experimental results. In summary, more scholars are currently using a two-dimensional heat transfer model to analyse the hot gas torch assisted AFP. Although the two-dimensional heat transfer model can significantly improve computational efficiency, it only gets the temperature distribution in two directions, which does not truly reflect the temperature field in the laying process. Meanwhile, the temperature distribution is calculated by modifying the convective heat transfer coefficient through an iterative process to make the simulation results consistent with the experimental results, which increases the simulation calculation time. In addition, there are fewer reports on hot gas torch assisted AFP three-dimensional heat transfer models, and the effect of nozzle geometry on the temperature distribution has not been considered in the reported literature.

Regarding the nozzle structure of the hot gas torch used for assisted AFP heating, there are usually circular structures and slit structures.[8,17] The temperature of the jet from a circular nozzle has an approximately Gaussian distribution, which causes an uneven temperature distribution in the heated area. In addition, the larger shape of the circular nozzle makes it impossible to get closer to the point of engagement. Compared to circular nozzles, slit nozzles provide a more uniform temperature distribution along the width of the pressure roller, which is currently used more in AFP heating.

A Slit Structure Nozzle Hot Gas Torch (SSNHGT) assisted AFP three-dimensional heat transfer model is constructed using the finite element method. Since this heating method is a convective heat transfer process, the temperature distribution of the hot air flow in the heated area of CF/PEEK thermoplastic composite is an important factor. Usually, the higher the temperature of the heat source the shorter the time it takes to heat CF/PEEK to the melting point. Therefore, the effect of gas flow rate and heat transfer distance on the hot air flow temperature distribution in the region near the point of engagement is analyzed to obtain the maximum temperature. Next, the temperature distribution of CF/PEEK heated at different laying speeds is analyzed using the maximum hot air flow temperature. Finally, orthogonal experiments and fuzzy grey relational analysis method are used to analyze the degree of influence of gas flow rate, heat transfer distance, and laying speed on the temperature distribution of CF/PEEK after being

heated, which can provide process optimization guidance for subsequent temperature control of CF/PEEK made by SSNHGT assisted AFP.

2. Numerical simulation and experimental methods

2.1. Numerical geometric model and boundary conditions

During the laying process, the hot air flow from the SSNHGT mainly heats the CF/PEEK tow near the engagement point. To improve the calculation efficiency of the numerical simulation, the three-dimensional heat transfer geometric model of the SSNHGT is obtained by simplifying the laying process, as shown in Fig. 1. Due to the narrow space to be heated, the effect of nozzle wall thickness on forced convection heat transfer cannot be ignored. The wall thickness of SSNHGT is 1 mm. Compared to rigid pressure rollers, flexible pressure rollers are used to ensure evenly distributed pressure on the prepreg during the laying process. The flexible pressure roller is mainly a high-hardness rubber sleeve on the outer surface of the steel roller. At the pressure of 0.5 MPa, the bottom of the flexible roller is deformed and the length of the contact surface with the mold is 21 mm. Other geometric model dimensions according to actual working conditions are shown in Fig. 1.

The boundary conditions of the simulation model and the thermal property parameters of the material are set according to the actual working conditions. The circular surface to the left of the nozzle is the velocity-inlet boundary condition, including the inlet temperature and velocity of the hot air. The inlet temperature is mainly determined by the gas flow rate, which is discussed in detail in Section 3.1.1. In the "trigonal" heating area on the right side of the geometric model, the two "triangular" surfaces and the rectangular surface on the left side are the pressure-outlet boundary conditions. The pressure outlet temperature is set to the default room temperature (25 °C). Since the curved surface of the pressure roller and the bottom mold surface are the main areas of interest to be heated, the convective heat exchange with air needs to be considered. They are set as non-slip wall boundary conditions that include convective heat transfer (5 $W/m^2 \cdot K$). The others remaining surfaces are set to non-slip adiabatic wall conditions since they are not the main object of interest. The types of heat source gases usually include compressed air or nitrogen, here we take compressed air as an example for numerical simulation. The thermal performance parameters of the material are shown in Table 1,[32] where the air is the ideal gas.

2.2. Grid division and irrelevance verification

In the numerical simulation calculation, the quantity and quality of the model grid have a great influence on the accuracy and precision of the simulation results. Grid refinement is usually applied to the computational region of interest in the model to improve computational accuracy. Therefore, the grid refinement of the pressure roller surface and the bottom mold

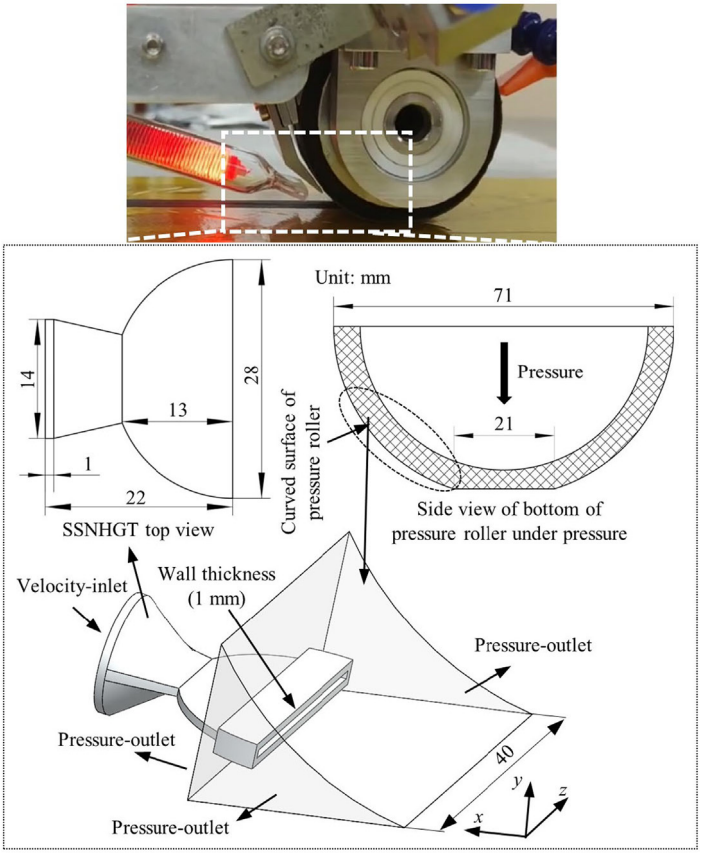

Fig. 1 Three-dimensional heat transfers geometric model of SSNHGT.

Table 1 Thermal performance parameters of materials.

Material	Density (kg/m^3)	Specific heat capacity (J/(kg·K))	Thermal conductivity (W/(m·K))	Glass transition (°C)	Melting point (°C)
Air		1006.43	0.0242		
CF/PEEK[32]	1560	1425	0.7	143	343

surface is performed to obtain an accurate temperature distribution. Due to the large variation of the hot air flow in the flat exit of the nozzle, it is also grid refined. Based on Fluent software, the final polyhedral mesh obtained is shown in Fig. 2(a).

In fact, it is not the case that the more the number of mesh elements is the better. According to the simulation practice experience, when the number of mesh elements increases to a certain degree, it has little effect on the final simulation results, but will seriously reduce the computational efficiency. Therefore, the number of mesh element should be reduced as much as possible while ensuring the accuracy of the simulation results. Using different mesh refinement parameters, the models with mesh elements numbers 721954, 1300077, 2142566, and 5496103 are obtained, respectively. The surface temperatures of different distances from the engagement point in x direction on the centerline of the pressure roller surface and the mold surface are obtained by simulations under the same conditions (inlet temperature of 800 °C, gas flow rate of 45 L/min, and heat transfer distance of 25 mm), as shown in Figs. 2(b) and (c). When the mesh element number is 721954, the results deviate seriously from several other simulation models. When the number of mesh elements reaches

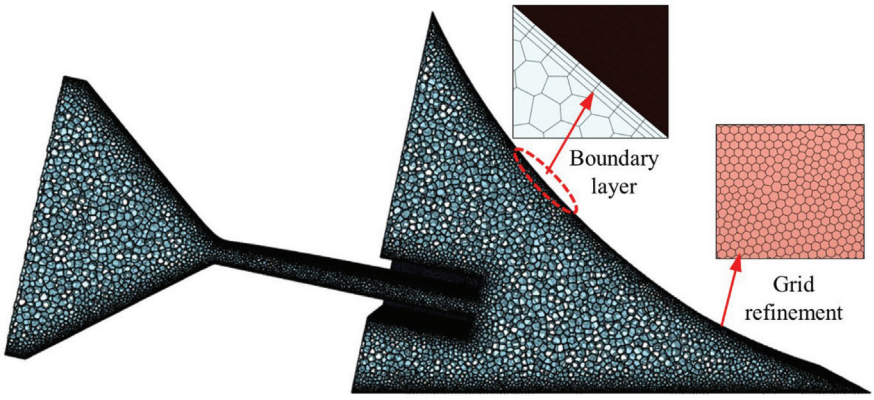

(a) Polyhedral mesh morphology

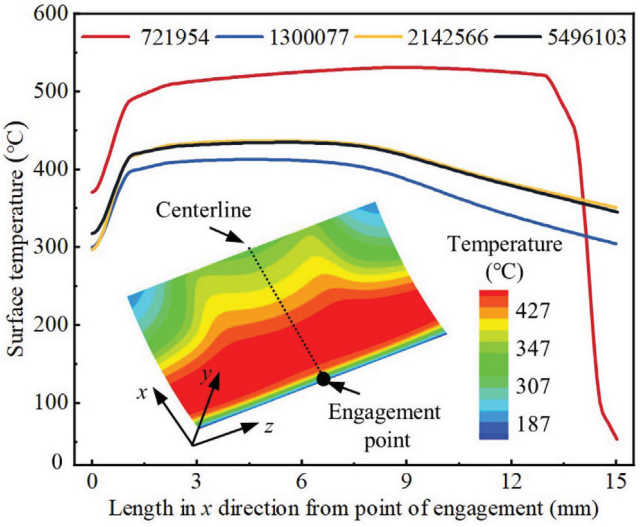

(b) Simulation results with different number of meshes on pressure roller surface

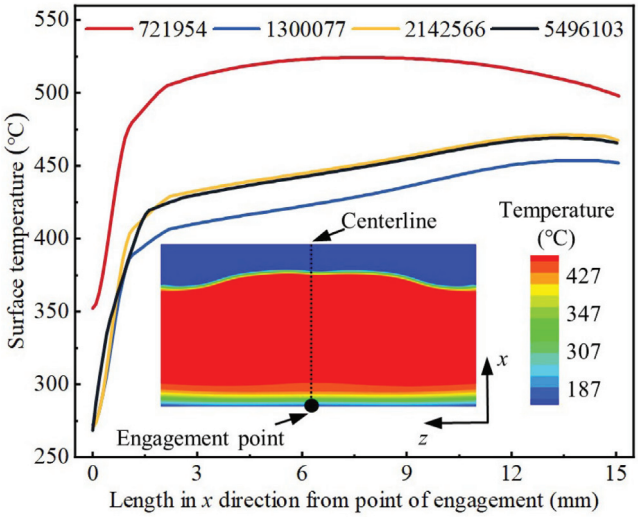

(c) Simulation results with different number of meshes on mold surface

Fig. 2 Polyhedral mesh and irrelevancy verification.

2×10^6, the simulation results are almost the same as 5×10^6, which indicates that the number of mesh elements in this simulation model needs to be up by at least 2×10^6.

2.3. Forced convection heat transfer control equation

SSNHGT assisted AFP three-dimensional heat transfer model is a forced convective heat transfer. Its control equations include the unsteady continuity equation (mass conservation), Navier-Stokes equation (momentum conservation), turbulence equation, and convective heat transfer equation.[33–36]

(1) Continuity equation

$$\frac{\partial}{\partial x_g}(\rho \bar{u}_g) = 0 \tag{1}$$

where x_g is spatial coordinate, $g = x, y, z$; ρ is the fluid density; $\bar{u}$ is the fluid time average velocity.

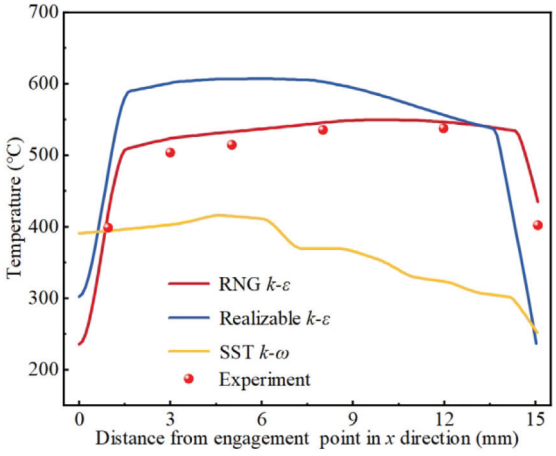

(a) Pressure roller surface

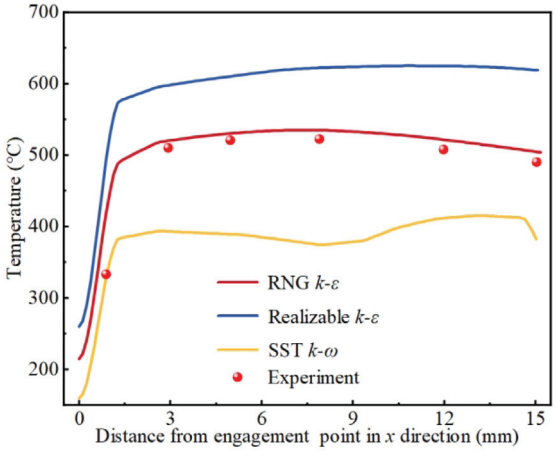

(b) Mold surface

Fig. 3 Comparison of three turbulence models.

(2) Navier-Stokes equation (take i direction as an example)

$$\frac{\partial}{\partial x_j}(\rho u_i u_j) = \frac{\partial p}{\partial x_i} + \frac{\partial}{\partial x_j}\left[(\mu + \mu_t)\left(\frac{\partial u_i}{\partial x_j} + \frac{\partial u_j}{\partial x_i}\right)\right] \tag{2}$$

where u is the velocity; p is the fluid time average pressure; μ is the fluid dynamic viscosity; μ_t is the fluid turbulent viscosity coefficient; i and j are the coordinate direction identifications.

(3) Turbulence equation

In forced convection simulation, two-equation turbulence models are generally used, such as SST k-ω model, RNG k-ε model, Realizable k-ε model, etc. Comparing the simulation results of the three turbulence models with the experimental results under the same parameters (the gas flow rate of 70 L/min, the heat transfer distance of 20 mm, and the wire laying speed of 0 mm/s), it is noticed from Fig. 3 that the results of the SST k-ω model are small, the results of the Realizable k-ε model are large, and the results of the RNG k-ε model are closed to the experimental results. Therefore, the RNG k-ε model is chosen in this heat transfer model.

The control equation of RNG k-ε model is

$$\frac{\partial(\rho k)}{\partial t} + \frac{\partial(\rho k u_i)}{\partial x_i} = \frac{\partial}{\partial x_j}\left(\alpha_k \mu_{\text{eff}} \frac{\partial k}{\partial x_j}\right) + G_k - \rho\varepsilon \tag{3}$$

$$\frac{\partial(\rho \varepsilon)}{\partial t} + \frac{\partial(\rho \varepsilon u_i)}{\partial x_i} = \frac{\partial}{\partial x_j}\left(\alpha_\varepsilon \mu_{\text{eff}} \frac{\partial \varepsilon}{\partial x_j}\right) + C_{1\varepsilon}^* \frac{\varepsilon}{k} G_k - C_{2\varepsilon}\rho \frac{\varepsilon^2}{k} \tag{4}$$

where

$$\begin{cases} \mu_{\text{eff}} = \mu + \mu_t \\ \mu_t = \rho C_u k^2/\varepsilon \\ C_u = 0.0845 \\ \alpha_k = \alpha_\varepsilon = 1.39 \\ C_{1\varepsilon}^* = C_{1\varepsilon} - \frac{\eta(1-\eta/\eta_0)}{1+\beta\eta^3} \\ \eta = (2E_{ij}E_{ij})^{1/2}\frac{k}{\varepsilon} \\ E_{ij} = \frac{1}{2}\left(\frac{\partial u_i}{\partial x_j} + \frac{\partial u_j}{\partial x_i}\right) \\ C_{1\varepsilon} = 1.42 \\ C_{2\varepsilon} = 1.68 \\ \eta_0 = 4.377 \\ \beta = 0.012 \end{cases} \tag{5}$$

where k is turbulent kinetic energy; t is the temperature; μ_{eff} is effective dynamic viscosity; ε is turbulent dissipation rate; G_k is shear generation term; η is kinetic viscosity; E_{ij} is i-row and j-column component of the turbulent stress tensor; the others are constants.

(4) Convective heat transfer equation

The main modes of heat transfer include heat radiation, heat convection, and heat conduction. In the Cartesian coordinate system, the differential form of the three-dimensional heat conduction equation without an internal heat source is generally expressed as

$$\rho c \frac{\partial t}{\partial \tau} = \frac{\partial}{\partial x}\left(\lambda \frac{\partial t}{\partial x}\right) + \frac{\partial}{\partial y}\left(\lambda \frac{\partial t}{\partial y}\right) + \frac{\partial}{\partial z}\left(\lambda \frac{\partial t}{\partial z}\right) \tag{6}$$

where λ, c, and τ are the thermal conductivity, specific heat capacity, and time of the thermal airflow micro-element, respectively.

The energy equation for convective heat transfer in this model is

$$\frac{\partial t}{\partial \tau}+u\frac{\partial t}{\partial x}+v\frac{\partial t}{\partial y}w\frac{\partial t}{\partial z}=\alpha\left(\frac{\partial^2 t}{\partial x^2}+\frac{\partial^2 t}{\partial y^2}+\frac{\partial^2 t}{\partial z^2}\right) \tag{7}$$

where u, v, and w are the velocity components along x, y, and z directions, respectively; α is the thermal diffusion coefficient, $\alpha = \lambda/(c\rho)$.

2.4. Experimental test method

The temperature testing experiments of SSNHGT assisted AFP are conducted on a four-filament bundle AFP machine developed by our team. It mainly includes the AFP system, gas supply system, and temperature measurement system, as shown in Fig. 4(a). The AFP system provides realistic working conditions for SSNHGT heating during the laying process. The air supply system provides a stable and dry compressed air flow, which is heated to a high temperature and blown out at high speed in the SSNHGT. Meanwhile, the flow rate is controlled by a gas flow meter. The temperature acquisition system selects the DC55 temperature inspection instrument produced by Zhongshan Zhongxiang Instrument Co., Ltd (China). The scanning speed is 100 ms–5 s, and the resolution is 0.1 °C. The reading temperature sampling rate is 1 time per second. The thermocouple is chosen as K type thermocouple with a temperature measurement range of 0–1000 °C. Meanwhile, the thermocouple is a custom armored thermocouple with a 1 mm diameter, a temperature tip of 50 mm long, and a response time of 0.1 s, which is tough enough to be used for temperature testing in narrow spaces.

The idea is obtaining the maximum heating temperature of the hot air flow by steady-state analysis first, followed by the temperature distribution of CF/PEEK being heated at different laying speeds using transient analysis when the hot air flow reaches the maximum temperature. When the thermocouple rotates with the pressure roller to measure the temperature, there are problems such as poor temperature measurement accuracy, difficult experimental operation, and easy damage of the thermocouple. Therefore, when the hot air flow reaches the maximum temperature, the parameters of gas flow rate and heat transfer distance can be easily obtained from the experimental under the steady-state analysis without considering the laying speed. However, in the process of steady-state analysis, it was found that the temperature of the hot air flow could reach 600 °C at certain parameters. This temperature already

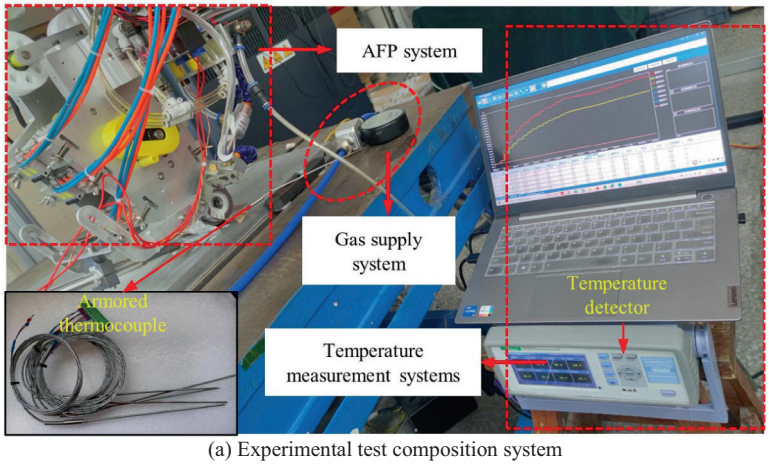

(a) Experimental test composition system

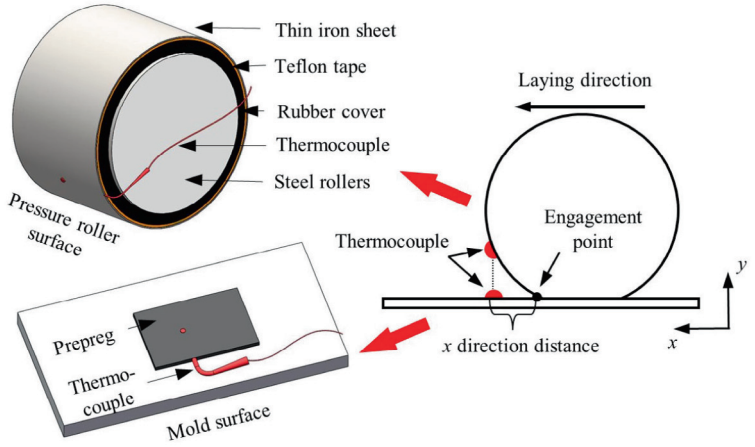

(b) Thermocouple installation location diagram

Fig. 4 Temperature test experiment.

exceeds the melting point of the rubber sleeve on the surface of the pressure roller. To ensure the experiment can be performed at high temperatures, multiple layers of high-temperature resistant Teflon tape are applied to the surface of the flexible pressure roller. The outermost layer is then covered with a layer of 0.15 mm thick iron sheet. When the laying speed is taken into consideration, the temperature of the hot gas flow will be controlled within the temperature range where CF/PEEK is heated and melted. At this moment, the outermost layer of the pressure roller does not need iron sheet protection, and the laying process conforms to the actual forming process. The thermocouple is fixed on the iron sheet for temperature measurement, where their position is in the middle of the pressure roller surface and the mold surface. Meanwhile, the thermocouples on both surfaces are in a vertical line along y direction, as shown in Fig. 4(b). During the experiment, the distance from the thermocouple to the engagement point in x direction is controlled by the movement of the robot arm, obtaining the temperature along x direction at different distances from the engagement point.

3. Results and discussion

3.1. Effect of single factor on temperature field

The factors affecting the temperature field of SSNHGT assisted AFP include the internal heat source temperature of the nozzle, gas flow rate, heat transfer distance, heat transfer angle, and laying speed. Heat source temperature and heat transfer angles are not analysed in this model because one of the engineering goals of using AFP to form composites is to increase production efficiency, which is to increase the laying speed. The laying speed is usually positively correlated with the heat source temperature. Therefore, this model sets the heat source temperature to 850 °C which is the maximum temperature allowed by the hot gas torch. The heat transfer angle is the angle between the line from the center point of the nozzle outlet to the point of engagement and the horizontal plane. Due to the narrow space to be heated, the range of adjustable heat transfer angle is small. Different heat transfer angles have less effect on the surface temperature of the pressure roller surface and the mold surface. Therefore, this model sets the heat transfer angle at 12°, which enables a minimum heat transfer distance of 15 mm at this angle and ensures a safe height of 5 mm from the lower edge of the nozzle outlet to the mold surface.

3.1.1. Gas flow rate

Before analyzing the temperature of the gas flow on the pressure roller surface and the mold surface, it is necessary to determine the inlet temperature in the velocity-inlet boundary condition. Because of the different gas flow rates in the hot gas torch, the compressed air is heated at different times, which leads to different inlet temperatures in the velocity-inlet boundary condition. However, the temperature variation inside the hot gas torch is difficult to obtain accurately by experiment. Therefore, numerical simulations are still used to obtain the inlet temperature at different gas flow rates. The specific methods are as follows:

Step 1 Construct a simulation model of the free jet in the air for the slit structure nozzle.

Step 2 Assuming an inlet temperature at a certain gas flow rate, the temperature at a position 1 mm from the center point of the nozzle outlet is calculated by simulation.

Step 3 The temperature at a position 1 mm from the center point of the nozzle outlet is obtained by experimental methods.

Step 4 The simulation results are compared with the experimental results for consistency to determine whether the set temperature of the velocity-inlet boundary condition is correct. If the results are the same, the assumed inlet temperature is the temperature of the velocity-inlet boundary condition at that gas flow rate. Otherwise, repeat Steps 1–4.

Fig. 5 shows the simulation model of the free jet in the air for the slit structure nozzle. The airflow field is constructed as a cylindrical area larger than the nozzle size to ensure complete coverage of the jet area. The selection of a cylindrical airflow field makes the grid division transition from the nozzle to the airflow field smoothly and facilitates the polyhedral grid division to improve the simulation accuracy. The grid division method is the same as described in Section 2.2. The final number of polyhedral mesh elements is 4735082. The airflow field boundary condition is set as pressure-outlet, the air is set as the ideal gas, and the turbulence model chose RNG k-ε. Using hot gas torch assisted AFP to form CF/PEEK composites, the gas flow rate of compressed air is generally in the range of 50–90 L/min.[17] In this model, the gas flow rates are selected as 30, 50, 70, 90, 110 L/min.

Fig. 6 shows the simulation and experiment results when the nozzle inlet temperatures are selected as 800, 755, 720, 670, 655 °C. The above inlet temperatures correspond to gas flow rates of 30, 50, 70, 90, 110 L/min, respectively. The simulation results of the jet temperature are taken from the data on the centerline within the symmetry plane in the model, as shown in Fig. 6(a). The temperature simulation results show a slight decrease in the airflow temperature inside the nozzle. Once the airflow leaves the nozzle, the jet temperature inside the air flow field drops sharply. Fig. 6(b) is the experimentally measured variation curve of the jet temperature with heating time at a position 1 mm from the nozzle exit center. At the beginning of the heating, jet temperature increases rapidly, then decreases and stabilizes. Because the SSNHGT uses a resistance wire to heat the compressed air, there is a short per-

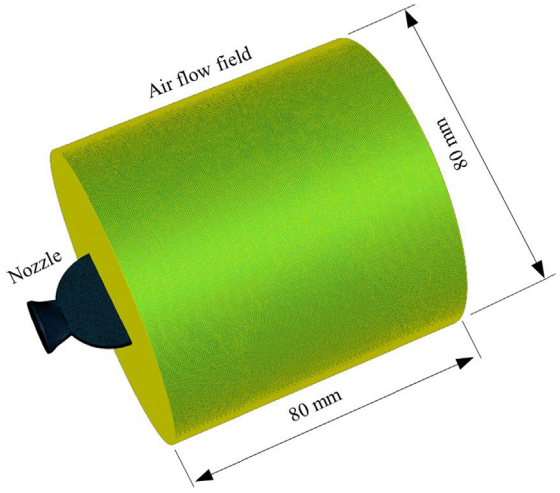

Fig. 5 Simulation model of free jet in air for slit structure nozzle.

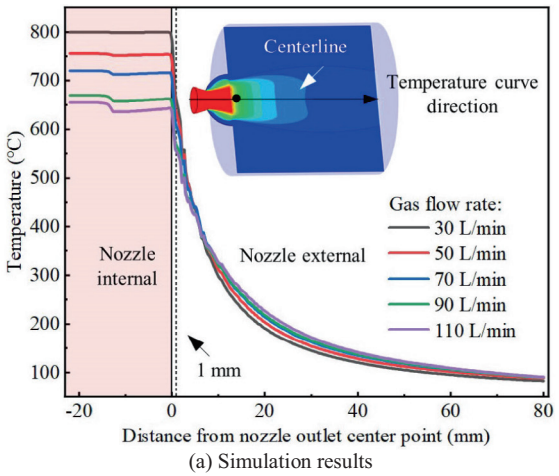

(a) Simulation results

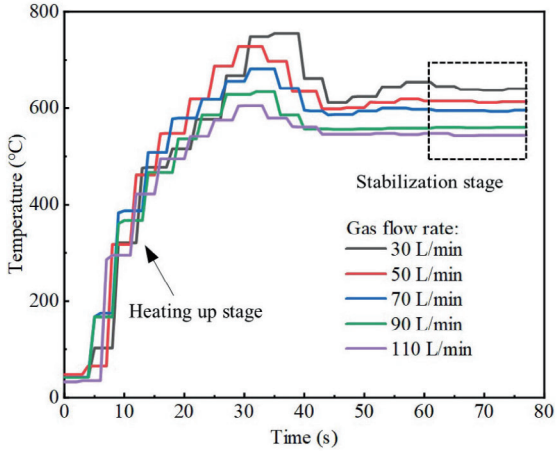

(b) Experimental results

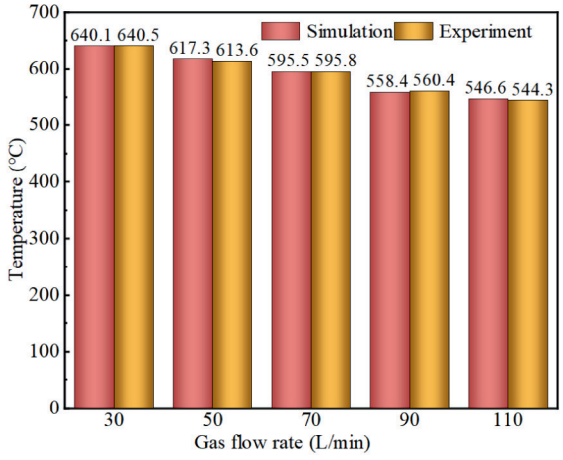

(c) Comparison between simulation and experimental results

Fig. 6 Simulation and experimental results of free jet at different gas flow rates.

iod of temperature overshoot when the resistance temperature is about to reach the set value. Subsequently, the resistance heating temperature stabilizes under closed-loop PID control. Therefore, the average of the last 10 s of the stable stage in the experimental test temperature curve is used as the final jet temperature. Fig. 6(c) is a comparison between the simulation results and the experimental results for the nozzle inlet temperature selected above for different gas flow rates, showing that the simulation results are almost consistent with the experimental results. Therefore, the boundary conditions of the nozzle inlet temperature at different gas flow rates are obtained.

The heat transfer distance is chosen as 20 mm and the laying speed is 0 mm/s. The temperature simulation results of the SSNHGT assisted AFP at different gas flow rates are obtained, as shown in Fig. 7. It can be noticed that hot gas vortexes are generated near the middle of the pressure roller surface and the mold surface, resulting in the highest temperature occurs at the location of the hot gas vortex. In addition, the hot air flow mainly rushes out to both sides (z direction) after impacting the pressure roller surface and mold surface, while the cold air around is mainly drawn into the hot air flow in y direction. As the gas flow rate increases, the heated area on the pressure roller surface and the mold surface changes from "rectangular" to "triangular". The overall temperature also tends to increase and then decrease. The temperature is higher in the gas flow rate range of 50–70 L/min.

Referring to the positions of the centerline and the engagement point in the pressure roller surface and mold surface in Fig. 2, the temperature simulation results in the range of 0–15 mm from the engagement point on the centerline in x direction at different gas flow rates are obtained, as shown in Fig. 8. The length of 15 mm is chosen because the projection of the line from the tow outlet to the engagement point on the horizontal plane is 15 mm. In addition, the simulation results are verified by experimentally measuring the temperature at positions 1, 3, 5, 8, 12, 15 mm from the engagement point. The experimental results are averaged over 10 s after the stabilization stage of the temperature curves. The experimental temperature curves tested are shown in Fig. S1 in Supplementary data. As can be seen in Fig. 8, the temperature obtained from the experiment at different gas flow rates is almost the same as the simulation results. However, the simulation results are slightly higher than the experimental results because the model established is a simplified ideal model, ignoring the heat transfer of other components in the AFP device. Meanwhile, by comparing the simulation result curves at different gas flow rates, it can be noticed that as the gas flow rate increases, the temperature near the engagement point (0 mm) is larger, which is due to the faster flow velocity of the higher gas flow rate, allowing the hot airflow to fully heat the area near the engagement point. However, the high gas flow rate lowers the nozzle inlet temperature, resulting in low temperatures in the area away from the engagement point. Therefore, the above analysis concludes that the gas flow rate in the range of 50–70 L/min can make the overall temperature of the pressure roller surface and the mold surface higher.

3.1.2. Heat transfer distance

The heat transfer distance is the straight-line distance from the center point of the nozzle outlet to the point of engagement. A minimum heat transfer distance of 15 mm is determined to avoid collision of the nozzle with the bottom mold during laying. The maximum heat transfer distance is chosen as 25 mm based on the pre-experiment of AFP forming CF/PEEK. The temperature distributions at heat transfer distances of 15, 17, 20, 23, 25 mm are obtained when the gas flow rate is 50 L/min and the laying speed is 0 mm/s, as shown in Fig. 9.

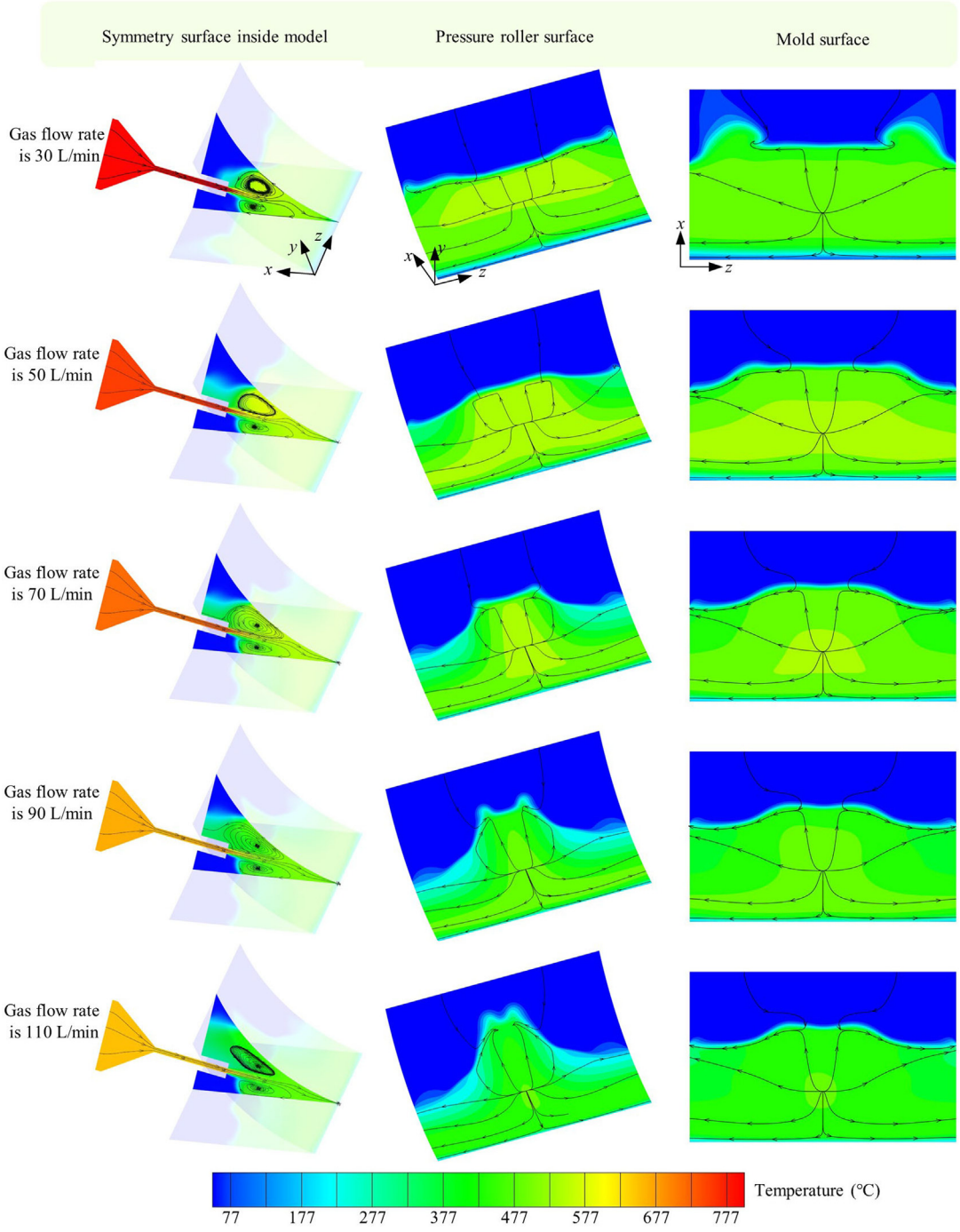

Fig. 7 Temperature distribution on pressure roller surface and mold surface at different gas flow rates.

For different heat transfer distances, hot gas vortices are also formed in the middle of the pressure roller surface and the mold surface, where the temperature is highest. Then, the hot gas flow rushes out to both sides in z direction. As the heat transfer distance increases, the range of the formed hot gas vortex becomes larger, making the area heated on the pressure roller surface and the mold surface increase. However, the temperature of the hot air flow is severely reduced.

Fig. 10 also shows the simulation and experimental results of the centerline on the pressure roller surface and the mold surface in the range from 0 to 15 mm in x direction from the engagement point. The experimental temperature curves tested are shown in Fig. S2 in Supplementary data. It can be seen from Fig. 10 that the experimental results are in good consistent with the laws of the simulation results. However, the experimental results are a little lower than the simulation results for the same reason as discussed in Section 3.1.1. As the heat transfer distance increases, the temperature in the area close to the engagement point (0 mm) on both the pressure roller surface and the mold surface decreases severely, while the temperature at the end far from the engagement point (15 mm) increases. Because the larger the heat transfer dis-

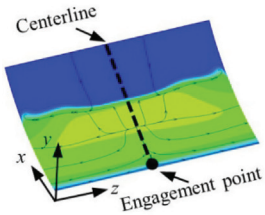

(a) Example of pressure roller surface

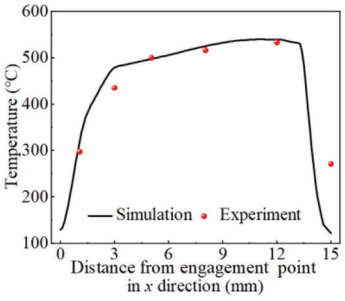

(a1) Pressure roller surface, gas flow rate is 30 L/min

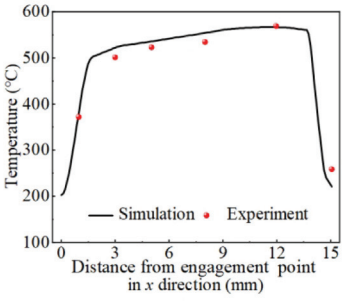

(a2) Pressure roller surface, gas flow rate is 50 L/min

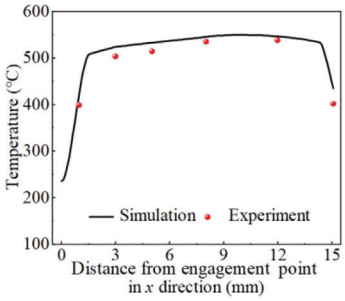

(a3) Pressure roller surface, gas flow rate is 70 L/min

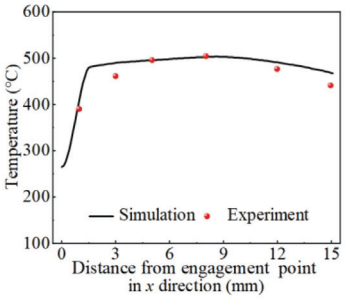

(a4) Pressure roller surface, gas flow rate is 90 L/min

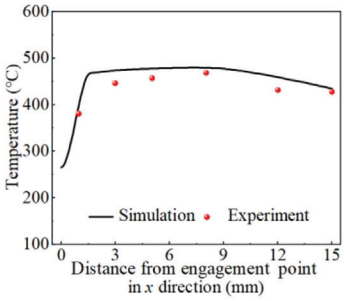

(a5) Pressure roller surface, gas flow rate is 110 L/min

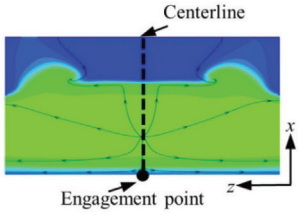

(b) Example of mold surface

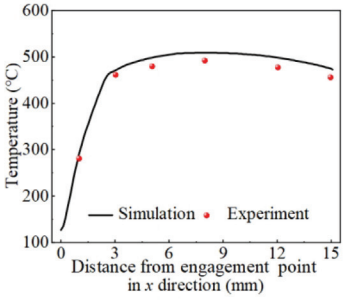

(b1) Mold surface, gas flow rate is 30 L/min

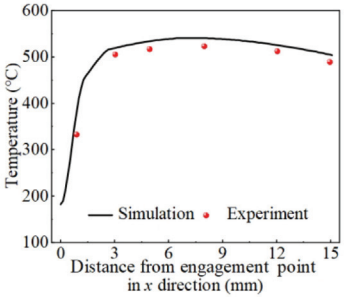

(b2) Mold surface, gas flow rate is 50 L/min

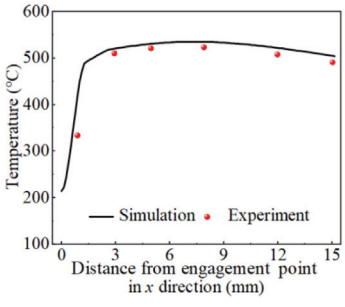

(b3) Mold surface, gas flow rate is 70 L/min

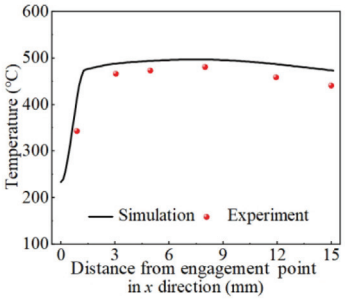

(b4) Mold surface, gas flow rate is 90 L/min

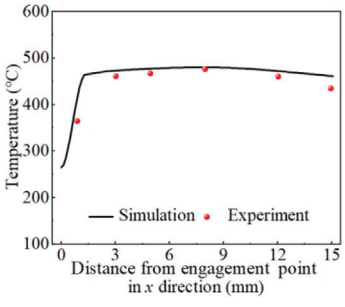

(b5) Mold surface, gas flow rate is 110 L/min

Fig. 8 Temperature distribution on centerline of pressure roller surface and mold surface at different gas flow rates.

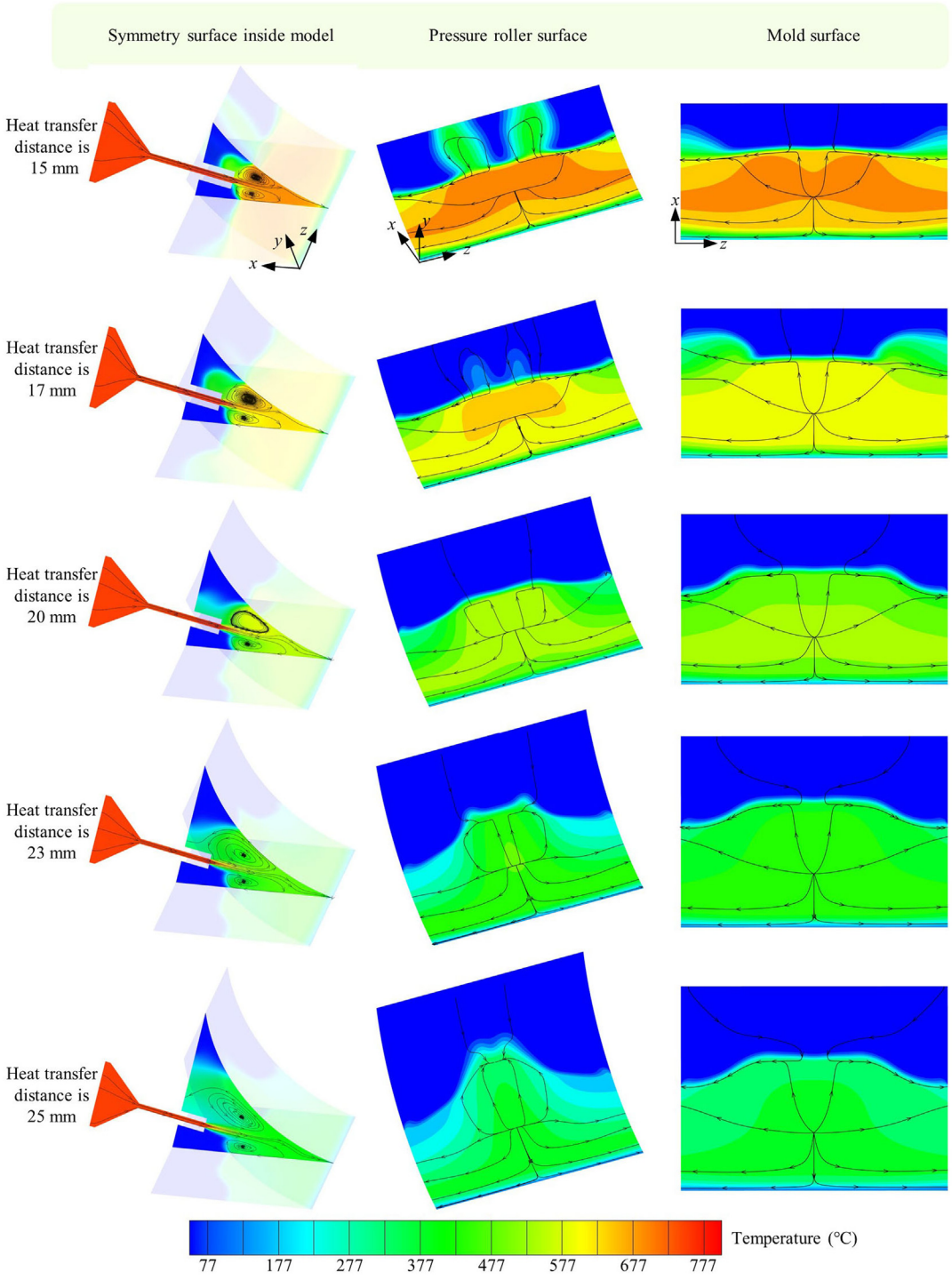

Fig. 9 Temperature distribution on pressure roller surface and mold surface at different heat transfer distances.

tance, the larger the range of the hot gas vortex formed, the larger the area heated on the pressure roller surface and the mold surface, resulting in the end away from the engagement point being able to be heated by more of the hot gas flow. Therefore, the end away from the engagement point is heated at a higher temperature, which is the opposite law of the gas flow rate. The above analysis shows that the heat transfer distance in the range of 17–23 mm can make the overall temperature on the pressure roller surface and the mold surface higher.

3.1.3. Laying speed

During the laying process, the laying speed significantly affects the heat transfer from the high-temperature jet to the CF/PEEK prepreg. In contrast to the steady-state simulation in Sections 3.1.1 and 3.1.2, where the laying speed is 0, the CF/PEEK movement speed needs to be setted for transient simulation. To improve the computational efficiency of transient simulation, the temperature distribution is simulated by the sliding mesh technique. The sliding mesh technique involves dividing the computational domain into multiple regions, each

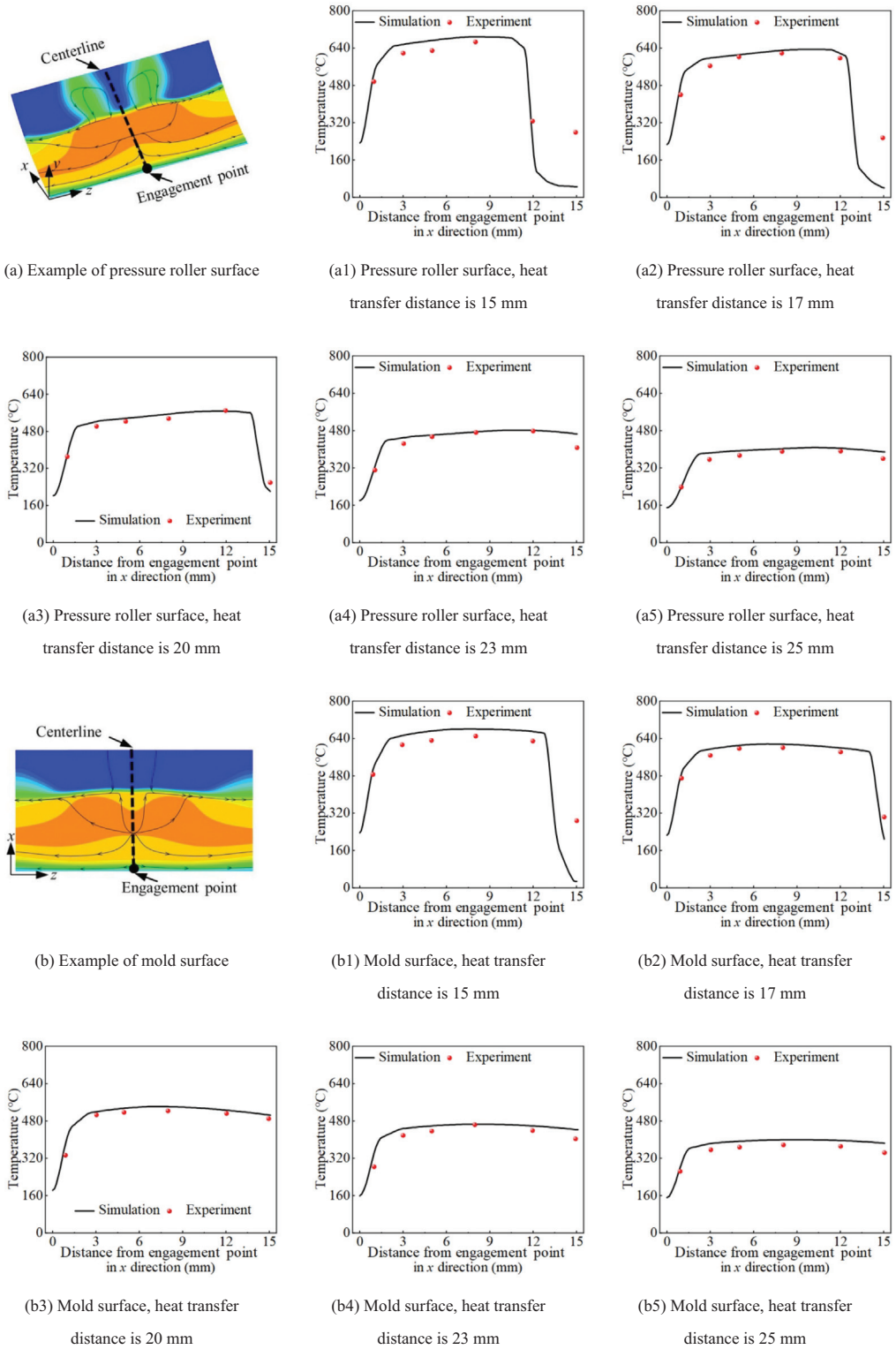

Fig. 10 Temperature distribution on centerline of pressure roller surface and mold surface at different heat transfer distances.

associated with a different moving component. These components may have different velocities and orientations. In addition, the sliding mesh technique allows data interaction between two computational regions while moving relative to each other. Meanwhile, it does not require interface mesh conodes and has the advantage of high computational efficiency for transient simulation.[37] Fig. 11(a) is the transient simulation model of the SSNHGT assisted AFP heating the CF/PEEK. The CF/PEEK with dimensions of 20 mm × 6.35 mm × 0.15 mm is set as a solid domain. The rest is the fluid domain.

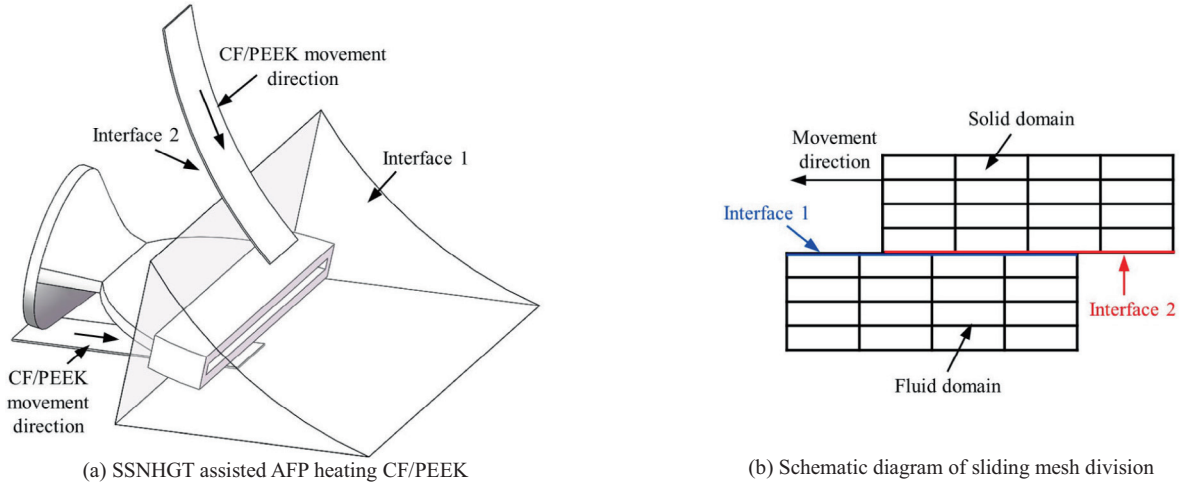

(a) SSNHGT assisted AFP heating CF/PEEK

(b) Schematic diagram of sliding mesh division

Fig. 11 Transient simulation model.

The intersection of solid and fluid domains is set as interface slip boundary conditions for data information transfer (as shown in Fig. 11(b)).

Fig. 12 is the temperature distribution of the CF/PEEK after being heated at lengths of 0, 3.6, 10.8, and 18.0 mm in x direction from the engagement point for laying speeds of 6, 8, 10, 12, and 15 mm/s, when the gas flow rate is 50 L/min and the heat transfer distance is 17 mm. The laying speed refers to the horizontal forward speed along x direction, while the CF/PEEK on the pressure roller surface needs to be converted into the angular speed of rotation. As can be seen from Fig. 12, the temperature of CF/PEEK moving to the same position decreases as the laying speed increases. When the CF/PEEK on the pressure roller surface and the mold surface reach the engagement point, both are heated to almost the same temperature. In addition, CF/PEEK is heated to 340 °C at a laying speed of 15 mm/s, which is slightly below its melting point of 343 °C. Therefore, the maximum laying speed for the SSNHGT assisted AFP forming CF/PEEK is 15 mm/s.

As can be seen in Fig. 12, the CF/PEEK is heated to its highest temperature when it moves to the engagement point position at different laying speeds. Therefore, as regards the experimental verification of the transient simulation results for different laying speeds, the thermocouple is mounted in the middle of the CF/PEEK prepreg on the mold surface (as shown in Fig. 4). The AFP is rolled over the thermocouple from the same position at different speeds, respectively. The output temperature is recorded by a highly sensitive temperature patrol, where the highest temperature recorded is the temperature near the point of engagement. However, the selected temperature patrol can only display data in real-time but cannot store temperature curve data. Therefore, the highest temperature picture is intercepted by video recording, as shown in Fig. 13(b). As can be seen from Fig. 13, the experimental results are consistent with the law of simulation results. The temperature of CF/PEEK after being heated decreases with increasing laying speed. Meanwhile, the experimental results are also slightly lower than the simulation results for the reasons described in Section 3.1.1. In the case of AFP rapid-forming CF/PEEK components, CF/PEEK is heated at 370–400 °C.[38] Therefore, the AFP laying speed is selected in the range of 8–12 mm/s.

3.2. Correlation analysis of various factors on CF/PEEK heated temperature

There is a high requirement for the heating temperature of the hot gas torch in the AFP rapid-forming CF/PEEK process. The control of the heating temperature usually requires a reasonable matching of different process parameters. Therefore, the orthogonal experiments and fuzzy grey relational analysis are used to evaluate the correlation of gas flow rate, heat transfer distance, and laying speed on the heated temperature of CF/PEEK, which guides the subsequent optimization of process parameters.

3.2.1. Orthogonal experimental design

The orthogonal experiment is an effective method based on probability theory and mathematical statistics when analysing the interaction effects of multiple factors on a system.[39] The $L_9(3^3)$ orthogonal experiment is designed using three factors and three levels according to the laws of gas flow, heat transfer distance, and laying speed on the temperature distribution in Section 3.1. Table 2 is the different factors and levels. The results of the orthogonal experiments are obtained using transient simulation because the laws of experimental and simulation results in the single-factor analysis are almost consistent. Table 3 is the results of the nine sets of orthogonal experiments.

Table 4 and Fig. 14 are the extreme difference analysis of gas flow rate, heat transfer distance, and laying speed on heating temperature. k_1, k_2, and k_3 are the response mean values of the temperature of the three factors at the three levels, respectively. The higher response means value of temperature indicates that the level is the superior level for the corresponding factor. R is the extreme difference of the response mean value of temperature, indicating the floating effect on the results when the level of a factor is changed. The larger the extreme difference, the greater the influence of the corresponding factor on the results. The gas flow rate has a maximum R of 99.0 °C, indicating that it has the greatest effect on the temperature, followed by the laying speed, and finally the heat transfer distance. It is visualized from Fig. 14 that the heating temperature increases with the increase of gas flow rate and decreases with the increase of heat transfer distance and laying

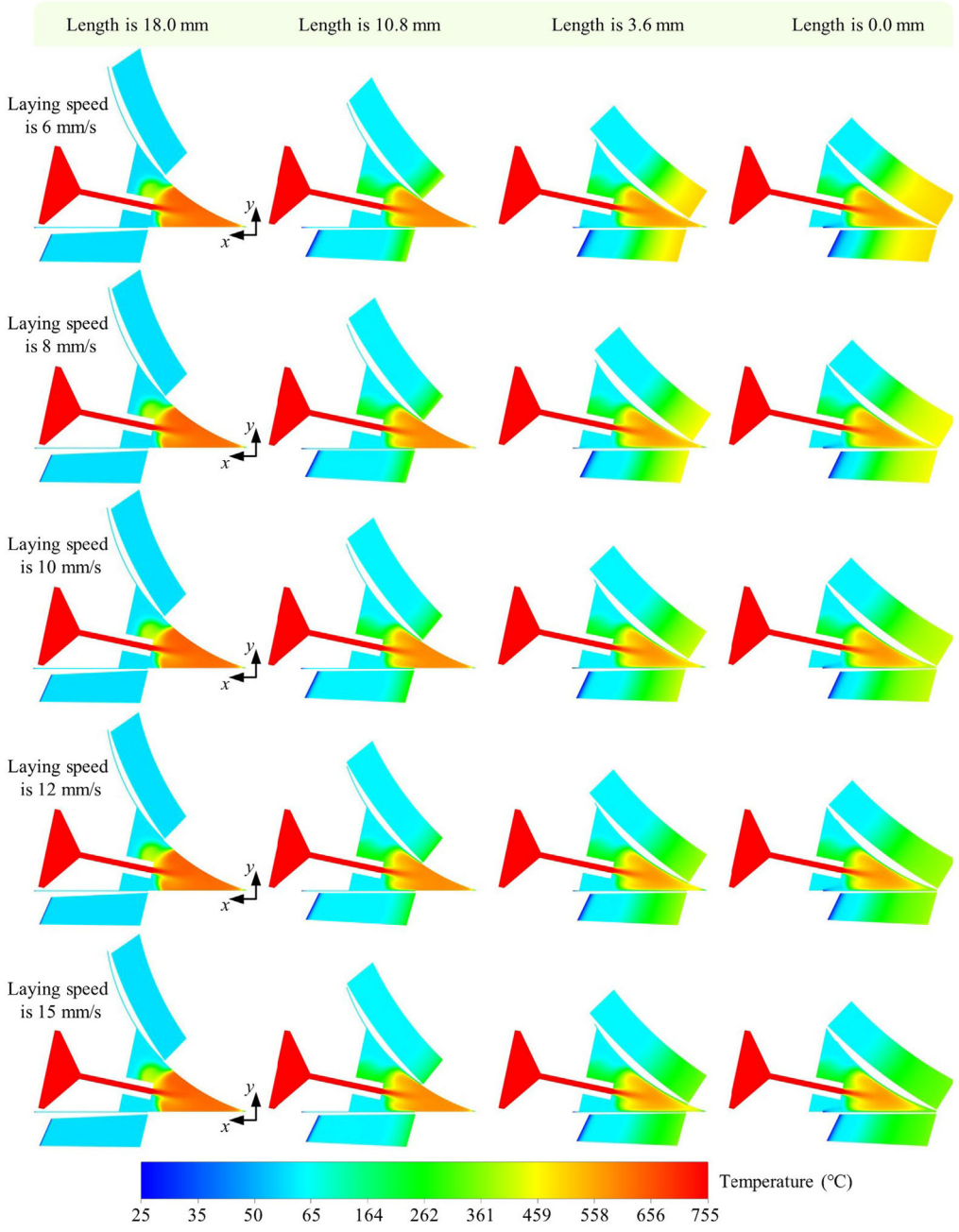

Fig. 12 Temperature distributions of CF/PEEK being heated at different laying speeds.

speed in the selected range of factors, which is consistent with the results of the single factor analysis.

3.2.2. *Fuzzy grey relational analysis*

Grey relational analysis is a statistical method for describing the development of multiple factors on the change of a characteristic of a system by quantitative comparison.[40] Its basic principle is to assess the closeness of association between indicators and factors by comparing their geometric similarity.[41] Based on the grey relevance, it is improved by using the fuzzy membership degree and Euclidean grey relational degree, which obtains the fuzzy grey relational degree results with higher accuracy.[42] The steps of the fuzzy grey relational analysis method are as follows:

Step 1 Determine the matrix of factors ($\boldsymbol{X}$) and indicators ($\boldsymbol{Y}$). The number of factors is assumed to be m and the number of experiments is n:

$$\begin{bmatrix} \boldsymbol{X} \\ \boldsymbol{Y} \end{bmatrix} = \begin{bmatrix} \boldsymbol{x}_1 \\ \boldsymbol{x}_2 \\ \vdots \\ \boldsymbol{x}_m \\ \boldsymbol{y}_i \end{bmatrix} = \begin{bmatrix} x_1(1) & x_1(2) & \cdots & x_1(n) \\ x_2(1) & x_2(2) & \cdots & x_2(n) \\ \vdots & \vdots & & \vdots \\ x_m(1) & x_m(2) & \cdots & x_m(n) \\ y_i(1) & y_i(2) & \cdots & y_i(n) \end{bmatrix}^{\mathrm{T}} \tag{8}$$

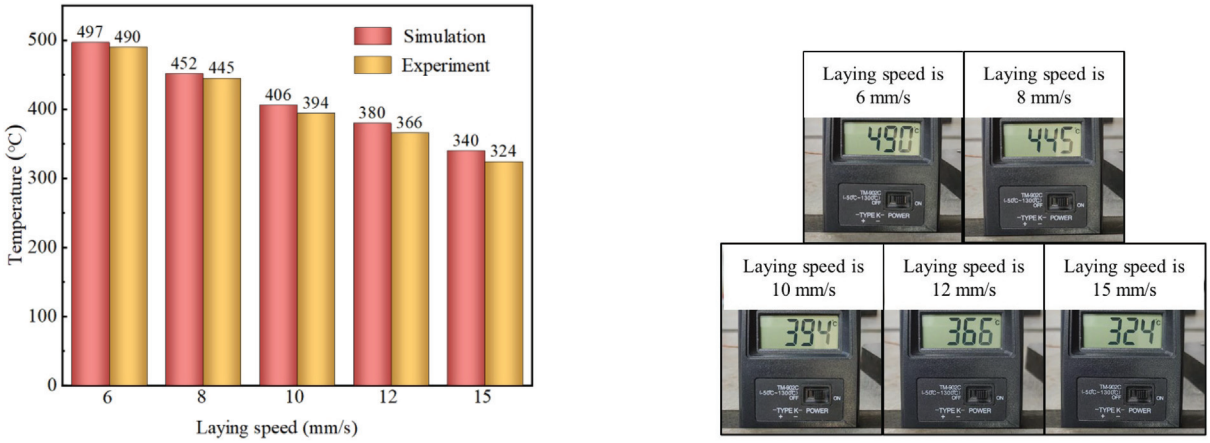

(a) Comparison of simulation and experimental results

(b) Highest temperatures of experimental test

Fig. 13 Simulation and experimental results at different laying speeds.

Table 2 Different factors and levels.

Level	Gas flow rate (L/min)	Heat transfer distance (mm)	Laying speed (mm/s)
1	30	17	8
2	50	20	10
3	70	23	12

Step 2 Normalize the matrix of factors and indicators:

$$x_i(k) = \frac{x_j(k) - \min x_j(k)}{\max x_j(k) - \min x_j(k)} \tag{9}$$

Step 3 Calculate the fuzzy membership degree r_1:

$$r_1 = \frac{\sum_{k=1}^{n} x(k)y(k)}{\sqrt{\sum_{k=1}^{n} x^2(k)}\sqrt{\sum_{k=1}^{n} y^2(k)}} \tag{10}$$

Step 4 Calculate the grey relational degree $\xi_i(k)$:

$$\xi_i(k) = \frac{\min|y_i(k) - x_i(k)| - p\max|y_i(k) - x_i(k)|}{|y_i(k) - x_i(k)| - p\max|y_i(k) - x_i(k)|} \tag{11}$$

where p is the grayscale resolution factor, usually taken as 0.5.

Step 5 Calculate the Euclidean grey relational degree r_2:

$$r_2 = 1 - \frac{1}{\sqrt{n}}\sqrt{\sum_{k=1}^{n}[1 - \xi_i(k)]^2} \tag{12}$$

Step 6 Calculate the fuzzy grey relational degree r. The closer the value of r to 1 indicates the stronger correlation between the factors and the indicators.

$$r = \sqrt{\frac{r_1^2 + r_2^2}{2}} \tag{13}$$

Based on the orthogonal experimental data in Table 3, the gas flow rate, heat transfer distance, and laying speed are used as the factor matrix and the temperature is used as the indicator matrix. The fuzzy membership degree, Euclidean grey relational, and fuzzy grey relational degree of gas flow rate, heat transfer distance and laying speed on temperature are calculated by Eqs. (8)–(13), respectively, as shown in Fig. 15. The results of fuzzy membership degree, Euclidean grey relational, and fuzzy grey relational degree for the gas flow rate are much greater than those for laying speed and heat transfer distance, indicating the gas flow rate has the greatest degree of influence on temperature, followed by laying speed and finally heat transfer distance. However, the results of the fuzzy grey relational analysis of laying speed and heat transfer distance are

Table 3 Results of orthogonal experiments.

No.	Level			Temperature (°C)
	Gas flow rate	Heat transfer distance	Laying speed	
1	1	1	1	344
2	1	2	2	294
3	1	3	3	263
4	2	1	2	413
5	2	2	3	364
6	2	3	1	375
7	3	1	3	440
8	3	2	1	462
9	3	3	2	356

Table 4 Results of analysis of extreme differences.

Factor	Temperature response mean value (°C)			
	k_1	k_2	k_3	R
Gas flow rate	300.3	384.0	399.3	99.0
Heat transfer distance	379.0	373.3	331.3	47.7
Laying speed	393.7	354.3	335.7	58.0

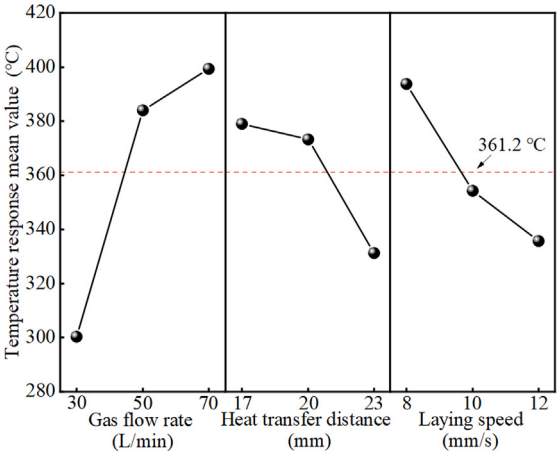

Fig. 14 Temperature response mean values.

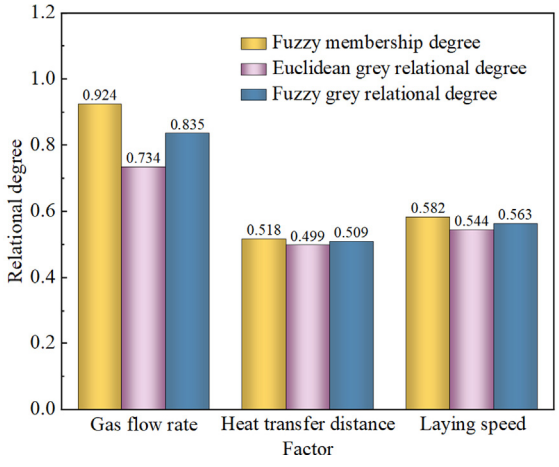

Fig. 15 Results of fuzzy grey relational analysis.

closer. Therefore, a parameter optimization strategy is provided for temperature field control in SSNHGT assisted AFP forming CF/PEEK thermoplastic composites. Since the heat transfer distance and laying speed have relatively little influence on the heating temperature, it is possible to determine the appropriate heat transfer distance and laying speed range first, and then adjust the gas flow rate mainly to achieve the target heating temperature. Using the maximum value in the heating temperature range (370–400 °C) of CF/PEEK thermoplastic composites formed by AFP as the optimization target, the optimal process parameters are obtained by orthogonal experiments and fuzzy grey relational analysis for a gas flow rate of 50 L/min, a laying speed of 10 mm/s, and a heat transfer distance of 17 mm, at which the CF/PEEK reaches the engagement point with a temperature of 394 °C.

4. Conclusions

(1) A three-dimensional heat transfer model for SSNHGT assisted AFP heating of CF/PEEK thermoplastic composites is created using the finite element method. The model can also be extended to other fiber-reinforced resin base composites formed by AFP using a hot gas torch with nozzles of other structures.

(2) The influencing factors of CF/PEEK heated by SSNHGT assisted AFP include gas flow rate, heat transfer distance, and laying speed. As the gas flow rate increases, the overall temperature increases and then decreases, while the temperature in the area near the engagement point increases. The overall temperature decreases as the heat transfer distance and laydown speed increase. However, when the heat transfer distance increases, the temperature increases in the end far from the engagement point.

(3) Through orthogonal experiments and fuzzy grey relational analysis, the gas flow rate has the greatest influence on the temperature of CF/PEEK being heated, followed by the laying speed and finally the heat transfer distance. The optimal process parameters are a gas flow rate of 50 L/min, a laying speed of 10 mm/s, and a heat transfer distance of 17 mm.

(4) Based on the results of the orthogonal experiment and fuzzy grey relational analysis, a process optimization scheme for heating temperature control is proposed. Firstly, the parameter ranges of laying speed and heat transfer distance are determined. Next, the heating temperature is controlled to reach the target value mainly by adjusting the magnitude of the gas flow rate.

Declaration of competing interest

The authors declare that they have no known competing financial interests or personal relationships that could have appeared to influence the work reported in this paper.

Acknowledgements

Ziang JIN and Shouzheng SUN contributed equally. This study was co-supported by the National Natural Science

Foundation of China (No. 52205460), the Heilongjiang Provincial Natural Science Foundation of China (No. LH2023E041). Ziang JIN thanks the support from the China Scholarship Council (CSC) to study abroad at the Nanyang Technological University.

Supplementary data

Supplementary data to this article can be found online at https://doi.org/10.1016/j.cja.2024.03.032.

References

1. Jin ZA, Han ZY, Chang C, et al. Review of methods for enhancing interlaminar mechanical properties of fiber-reinforced thermoplastic composites: Interfacial modification, nano-filling and forming technology. *Compos Sci Technol* 2022;**228**:109660.
2. Peeters D, Jones D, O'Higgins R, et al. Experimental quality assessment of thermoplastic composite corner regions manufactured using laser-assisted tape placement. *Compos Struct* 2022;**297**:115911.
3. Alves de Campos A, Henriques E, Magee CL. Technological improvement rates and recent innovation trajectories in automated advanced composites manufacturing technologies: A patent-based analysis. *Compos Part B Eng* 2022;**238**:109888.
4. Sun SZ, Han ZY, Fu HY, et al. Defect characteristics and online detection techniques during manufacturing of FRPs using automated fiber placement: A review. *Polymers* 2020;**12**(6):1337.
5. Donough MJ, Shafaq, St John NA, et al. Process modelling of In-situ consolidated thermoplastic composite by automated fibre placement–A review. *Compos Part A Appl Sci Manuf* 2022;**163**:107179.
6. Sun SZ, Jin ZA, Liu XL, et al. *In situ* consolidation process-based fabrication and interlaminar modification mechanism associated with CF/PEEK multiscale nanocomposites characterized by interlaminar doping of CNTs. *Compos Sci Technol* 2022;**222**:109356.
7. Jin ZA, Han ZY, Liu XL, et al. The interlaminar performance of carbon fiber reinforced polyetheretherketone composites reinforced by doped buckypaper. *Mater Lett* 2022;**321**:132426.
8. Qureshi Z, Swait T, Scaife R, et al. *In situ* consolidation of thermoplastic prepreg tape using automated tape placement technology: Potential and possibilities. *Compos Part B Eng* 2014;**66**:255–67.
9. Comer AJ, Ray D, Obande WO, et al. Mechanical characterisation of carbon fibre–PEEK manufactured by laser-assisted automated-tape-placement and autoclave. *Compos Part A Appl Sci Manuf* 2015;**69**:10–20.
10. Bandaru AK, Clancy G, Peeters D, et al. Properties of a thermoplastic composite skin-stiffener interface in a stiffened structure manufactured by laser-assisted tape placement with *in situ* consolidation. *Compos Struct* 2019;**214**:123–31.
11. Stokes-Griffin CM, Compston P. The effect of processing temperature and placement rate on the short beam strength of carbon fibre–PEEK manufactured using a laser tape placement process. *Compos Part A Appl Sci Manuf* 2015;**78**:274–83.
12. Oromiehie E, Gangadhara Prusty B, Compston P, et al. In-situ simultaneous measurement of strain and temperature in automated fiber placement (AFP) using optical fiber Bragg grating (FBG) sensors. *Adv Manuf Polym Compos Sci* 2017;**3**(2):52–61.
13. Peeters D, Deane M, O'Higgins R, et al. Morphology of ply drops in thermoplastic composite materials manufactured using laser-assisted tape placement. *Compos Struct* 2020;**251**:112638.
14. Venkatesan C, Velu R, Vaheed N, et al. Effect of process parameters on polyamide-6 carbon fibre prepreg laminated by IR-assisted automated fibre placement. *Int J Adv Manuf Technol* 2020;**108**(4):1275–84.
15. Kollmannsberger A, Lichtinger R, Hohenester F, et al. Numerical analysis of the temperature profile during the laser-assisted automated fiber placement of CFRP tapes with thermoplastic matrix. *J Thermoplast Compos Mater* 2018;**31**(12):1563–86.
16. Zacherl L, Shadmehri F, Rother K. Determination of convective heat transfer coefficient for hot gas torch (HGT)-assisted automated fiber placement (AFP) for thermoplastic composites. *J Thermoplast Compos* 2023;**36**(1):73–95.
17. Aghababaei Tafreshi O, Van Hoa S, Shadmehri F, et al. Determination of convective heat transfer coefficient for automated fiber placement (AFP) for thermoplastic composites using hot gas torch. *Adv Manuf Polym Compos Sci* 2020;**6**(2):86–100.
18. Shadmehri F, Hoa SV, Fortin-Simpson J, et al. Effect of in situ treatment on the quality of flat thermoplastic composite plates made by automated fiber placement (AFP). *Adv Manuf Polym Compos Sci* 2018;**4**(2):41–7.
19. Oromiehie E, Gain AK, Prusty BG. Processing parameter optimisation for automated fibre placement (AFP) manufactured thermoplastic composites. *Compos Struct* 2021;**272**:114223.
20. Oromiehie E, Gain AK, Donough MJ, et al. Fracture toughness assessment of CF-PEEK composites consolidated using hot gas torch assisted automated fibre placement. *Compos Struct* 2022;**279**:114762.
21. Tierney J, Gillespie JW. Modeling of heat transfer and void dynamics for the thermoplastic composite tow-placement process. *J Compos Mater* 2003;**37**(19):1745–68.
22. Pitchumani R, Ranganathan S, Don RC, et al. Analysis of transport phenomena governing interfacial bonding and void dynamics during thermoplastic tow-placement. *Int J Heat Mass Transf* 1996;**39**(9):1883–97.
23. Beyeler EP, Güçeri SI. Thermal analysis of laser-assisted thermoplastic-matrix composite tape consolidation. *J Heat Transf* 1988;**110**(2):424–30.
24. Sonmez FO, Hahn HT. Modeling of heat transfer and crystallization in thermoplastic composite tape placement process. *J Thermoplast Compos Mater* 1997;**10**(3):198–240.
25. Kim HJ, Kim SK, Lee WI. Flow and heat transfer analysis during tape layup process of APC-2 prepregs. *J Thermoplast Compos Mater* 2004;**17**(1):5–12.
26. Tierney J. Modeling of *in situ* strength development for the thermoplastic composite tow placement process. *J Compos Mater* 2006;**40**(16):1487–506.
27. Toso YMP, Ermanni P, Poulikakos D. Thermal phenomena in fiber-reinforced thermoplastic tape winding process: Computational simulations and experimental validations. *J Compos Mater* 2004;**38**(2):107–35.
28. Li ZM, Yang T, Du Y. Dynamic finite element simulation and transient temperature field analysis in thermoplastic composite tape lay-up process. *J Thermoplast Compos Mater* 2015;**28**(4):558–73.
29. Tafreshi OA, Van Hoa S, Shadmehri F, et al. Heat transfer analysis of automated fiber placement of thermoplastic composites using a hot gas torch. *Adv Manuf Polym Compos Sci* 2019;**5**(4):206–23.
30. Moghadamazad M, Hoa SV. Models for heat transfer in thermoplastic composites made by automated fiber placement using hot gas torch. *Compos Part C Open Access* 2022;**7**:100214.
31. Hassan N, Thompson JE, Batra RC, et al. A heat transfer analysis of the fiber placement composite manufacturing process. *J Reinf Plast Compos* 2005;**24**(8):869–88.
32. Cao ZL, Dong MJ, Liu KL, et al. Temperature field in the heat transfer process of PEEK thermoplastic composite fiber placement. *Materials* 2020;**13**(19):4417.
33. Afroz F, Sharif MAR. Numerical study of heat transfer from an isothermally heated flat surface due to turbulent twin oblique confined slot-jet impingement. *Int J Therm Sci* 2013;**74**:1–13.

34. Chang-geng L, Jie-min Z. Experimental and numerical simulation study of heat transfer due to confined impinging circular jet. *Chem Eng & Technol* 2007;**30**(10):1355–61.
35. Huang HK, Sun TZ, Zhang GY, et al. Modeling and computation of turbulent slot jet impingement heat transfer using RANS method with special emphasis on the developed SST turbulence model. *Int J Heat Mass Transf* 2018;**126**:589–602.
36. Pakhomov MA, Terekhov VI. The effect of confinement on the flow and turbulent heat transfer in a mist impinging jet. *Int J Heat Mass Transf* 2011;**54**(19–20):4266–74.
37. ANSYS Inc. Academic research user guide (in release 12.0). Available from: https://www.afs.enea.it/project/neptunius/docs/fluent/html/th/node37.htm.
38. Çelik O, Peeters D, Dransfeld C, et al. Intimate contact development during laser assisted fiber placement: Microstructure and effect of process parameters. *Compos Part A Appl Sci Manuf* 2020;**134**:105888.
39. Zuo W, Jiaqiang E, Liu X, et al. Orthogonal experimental design and fuzzy grey relational analysis for emitter efficiency of the micro-cylindrical combustor with a step. *Appl Therm Eng* 2016;**103**:945–51.
40. Kadier A, Abdeshahian P, Simayi Y, et al. Grey relational analysis for comparative assessment of different cathode materials in microbial electrolysis cells. *Energy* 2015;**90**:1556–62.
41. Lv HL, Chen XY, Wang XY, et al. A novel study on a micromixer with Cantor fractal obstacle through grey relational analysis. *Int J Heat Mass Transf* 2022;**183**:122159.
42. He LF, Tang XW, Luo QL, et al. Structure optimization of a heat pipe-cooling battery thermal management system based on fuzzy grey relational analysis. *Int J Heat Mass Transf* 2022;**182**:121924.